Inorg. Chem. **2003**, *42*, 4382–4388

Synthesis and Characterization of N_2S_3X–Fe Models of Iron-Containing Nitrile Hydratase

Craig A. Grapperhaus,*,† Ming Li,† Apurba K. Patra,† Selma Poturovic,† Pawel M. Kozlowski,† Marek Z. Zgierski,‡ and Mark S. Mashuta†

Department of Chemistry, University of Louisville, Louisville, Kentucky 40292, and ‡Steacie Institute for Molecular Science, National Research Council of Canada, Ottawa, Ontario, Canada K1A OR6

Received December 5, 2002

A series of iron complexes based on the pentadentate ligand 4,7-bis(2′-methyl-2′-mercaptopropyl)-1-thia-4,7-diazacyclononane), $(bmmp\text{-}TASN)^{2-}$, have been synthesized and characterized as models of iron-containing nitrile hydratase (NHase). The chloro derivative $[(bmmp\text{-}TASN)Fe^{III}Cl]\cdot 0.5EtOH$ (**1**) contains a labile chloride which facilitates synthesis of related complexes via substitution reactions. Complex **1** is high-spin, $g = 4.28$. Addition of NEt_4CN with **1** in CH_2Cl_2 results in the cyanide ligated complex $[(bmmp\text{-}TASN)Fe^{III}CN]\cdot 0.5EtOH$ (**2**), which shows a single intense ν_{CN} band at 2083 cm^{-1} in the IR region. Complex **2** is low-spin, $g_1 = 2.31$, $g_2 = 2.16$, and $g_3 = 1.96$. Under basic conditions complex **1** affords a μ-oxo bridged dimeric Fe(III) complex $[(bmmp\text{-}TASN)Fe^{III}]_2O$ (**3**), which shows an intense band at 799 cm^{-1}. Complex **3** was recrystallized from CH_2Cl_2/hexane solution in the triclinic space group $P\bar{1}$, with $a = 10.5486(15)$ Å, $b = 13.0612(19)$ Å, $c = 8.1852(12)$ Å, $\alpha = 96.923(2)°$, $\beta = 112.729(2)°$, $\gamma = 81.048(2)°$, and $Z = 1$. Density functional theory (DFT) calculations of the previously communicated iron–nitrosyl complex $[(bmmp\text{-}TASN)Fe^{III}(NO)][BPh_4]$ (**4**) (*Inorg. Chem.* **2002**, *41*, 1039–1041) reveal that the HOMO region is dominated by Fe–S bonding. Complexes **1**–**4** display irreversible or quasi-reversible reductions in the cyclic voltammograms. All of the iron complexes and the zinc derivative, (bmmp-TASN)Zn (**5**), display an irreversible oxidation. Complex **5** was crystallized in the monoclinic space group $P2_1/n$ with $a = 9.5759(6)$ Å, $b = 20.9790(13)$ Å, $c = 10.7113(7)$ Å, $\beta = 91.283(1)°$, and $Z = 4$.

Introduction

The enzyme nitrile hydratase (NHase) incorporates non-heme iron(III) or non-corrin cobalt(III) for the catalytic hydrolysis of nitriles to amides.[1−5] Microbial NHase functions as a successful biocatalyst for the kiloton-scale production of acrylamide and nicotinamide in Japan[3,6,7] and in the bioremediation of agricultural (herbicidal) and industrial wastewater.[8−11] The active site of iron-containing NHase contains a low-spin, iron(III) ion in an N_2S_3X core. Endogenous nitric oxide inactivates the enzyme upon aerobic incubation in the dark. Photolysis restores activity suggesting an NO-photoregulatory mechanism.[12−15]

* E-mail: grapperhaus@louisville.edu.
† University of Louisville.
‡ National Research Council of Canada.

(1) Kobayashi, M.; Shimizu, S. *Nat. Biotechnol.* **1998**, *16*, 733−736.
(2) Kobayashi, M.; Shimizu, S. *Eur. J. Biochem.* **1999**, *261*, 1−9.
(3) Kobayashi, M.; Nagasawa, T.; Yamada, H. *Trends Biotechnol.* **1992**, *10*, 402−408.
(4) Brennan, B. A.; Alms, G.; Nelson, M. J.; Durney, L. T.; Scarrow, R. C. *J. Am. Chem. Soc.* **1996**, *118*, 9194−9195.
(5) Artaud, I.; Chatel, S.; Chauvin, A. S.; Bonnet, D.; Kopf, M. A.; Leduc, P. *Coord. Chem. Rev.* **1999**, *192*, 577−586.
(6) Yamada, H.; Kobayashi, M. *Biosci., Biotechnol., Biochem.* **1996**, *60*, 1391−1400.
(7) Nagasawa, T.; Yamada, H. *Trends Biotechnol.* **1989**, *7*, 153−158.
(8) Battistel, E.; Bernardi, A.; Maestri, P. *Biotechnol. Lett.* **1997**, *19*, 131−134.
(9) Wyatt, J. M.; Knowles, C. J. *Int. Biodeterior. Biodegrad.* **1995**, 227−248.
(10) Stalker, D. M.; McBride, K. E.; Malyj, L. D. *Science* **1988**, *242*, 419−423.
(11) Stalker, D. M.; Kiser, J. A.; Baldwin, G.; Coulombe, B.; Houk, C. M. In *Herbicide Resistant Crops*; Duke, S. O., Ed.; Lewis Publishers: New York, 1996; pp 93−105.
(12) Nagamune, T.; Kurata, H.; Hirata, M.; Honda, J.; Hirata, A.; Endo, I. *Photochem. Photobiol.* **1990**, *51*, 87−90.
(13) Noguchi, T.; Honda, J.; Nagamune, T.; Sasabe, H.; Inoue, Y.; Endo, I. *FEBS Lett.* **1995**, *358*, 9−12.
(14) Bonnet, D.; Artaud, I.; Moali, C.; Petre, D.; Mansuy, D. *FEBS Lett.* **1997**, *409*, 216−220.
(15) Odaka, M.; Fujii, K.; Hoshino, M.; Noguchi, T.; Tsujimura, M.; Nagashima, S.; Yohda, M.; Nagamune, T.; Inoue, Y.; Endo, I. *J. Am. Chem. Soc.* **1997**, *119*, 3785−3791.

10.1021/ic026239t CCC: $25.00
Published on Web 06/17/2003

X-ray crystal structures of the active and NO-inactivated forms of Fe-NHase have been reported at 2.65 Å[16] and 1.7 Å[17] resolution, respectively. The lower resolution, active state from *Rhodococcus sp.* R312 shows the unusual coordination of two amido nitrogens from the protein backbone, three cysteine thiolate sulfurs, and a sixth, nonprotein ligand, presumably hydroxide or water.[16] The higher resolution, NO-inactivated state from *Rhodococcus sp.* N-771 confirms the gross Fe-core structure and reveals that two of the cysteines have been modified resulting in a *mixed thiolato (RS^-), sulfenato ($RS(O)^-$), sulfinato (RSO_2^-) donor set*.[17,18] Notably, sulfur oxygenation could not be delineated at resolutions less than 2.3 Å consistent with their absence in the lower resolution report.[17] NO occupies the site trans to the unmodified cysteine. Additionally, Fe-NHase prepared under anaerobic conditions from recombinant subunits lack activity and characteristic S-oxygenate peaks in the mass spectrum.[19] Oxygen exposure instates activity, at which time S-oxygenation is evident in the mass spectrum.[19] That observation strongly suggests that *posttranslational modification of cysteine is required for hydratase activity*.[19] Recent theoretical investigations are consistent with an S-oxygenation requirement for photoreactivity of NO-inactivated NHase.[20]

While protein sulfenic acids are known to serve in redox regulation and/or redox catalysis, what role the oxygenated cysteine residues play in the catalytic cycle of NHase remains to be determined.[21] The current status of NHase models has recently been reviewed.[5,22] Several groups have employed N_3S_2 models, including amido-thiolates,[23−26] imino-thiolates,[27−31] or amino-thiolates,[32] to mimic the N_2S_3 donor environment of NHase. Less work with N_2S_3 ligands has been reported.[5] In the current study, we report a series of complexes based on the N_2S_3 pentadentate ligand, (bmmp-TASN)$^{2-}$. The ligand coordinates iron via a facially capping TASN ring and two pendant thiolato arms cis to one another. This reproduces, to a first approximation, the first coordination sphere of iron in the enzyme as we have previously reported in communication form.[33]

Experimental Section

Materials and Reagents. All chemicals were obtained from commercial sources and used as received unless otherwise noted. $[Bu_4N][FeCl_4]$ was prepared from equimolar amounts of Bu_4NCl and $FeCl_3$ in ethanol. Isobutylene sulfide was prepared according to literature methods and stored under N_2 at −20 °C.[34] 1-Thia-4,7-diazacyclononane (TASN) was prepared according to the method of Hoffmann et al.[35] [(bmmp-TASN)FeNO]BPh_4 (**4**) was prepared as previously reported.[33] Solvents were purified and dried following conventional drying procedures and freshly distilled prior to use. Reactions were carried out under nitrogen atmosphere at room temperature, unless otherwise specified.

***N,N′*-Bis-(2-methyl-2-mercaptopropyl)-1-thia-4,7-diazacyclononane (H_2bmmp-TASN).** To 1-thia-4,7-diazacyclononane (TASN) (0.50 g, 3.4 mmol) in a Schlenk flask under nitrogen was added isobutylene sulfide (6.0 g, 68 mmol) via syringe. The reaction mixture was stirred for 3 days at 70 °C under nitrogen in a sealed flask. Removal of excess isobutylene sulfide under vacuum yielded a colorless oil, which was used immediately or converted to the HCl salt. Yield: 0.79 g (73%).

[(bmmp-TASN)Fe^{III}Cl]·0.5EtOH (1). Freshly prepared H_2-bmmp-TASN (0.79 g, 3.3 mmol) was dissolved in dry, degassed ethanol (30 mL). Subsequently, an ethanol solution (10 mL) of NEt_3 (0.68 g, 6.7 mmol) was added via cannula. To the stirred ligand was added $[Bu_4N][FeCl_4]$ (1.36 g, 3.10 mmol) in ethanol (20 mL). A deep blue precipitate immediately formed, and the resulting reaction mixture was stirred overnight under N_2 atmosphere. The dark blue solid was isolated by filtration and washed with dry, degassed ethanol (150 mL) and ether (50 mL) and vacuum-dried. Yield: 1.46 g (94%). Electronic absorption spectra: (CH_2Cl_2) λ_{max} (ϵ_M) = 631 (5680), 457 (2510), 321 (11500), 230 (12500) nm. IR (KBr) ν (cm^{-1}): 3438 (alcohol −OH). Anal. Calcd for $C_{15}H_{31}N_2S_3O_{0.5}FeCl$: C, 41.47; H, 7.08; N, 6.45. Found: C, 42.57; H, 6.88; N, 6.43.

[(bmmp-TASN)Fe^{III}CN]·0.5EtOH (2). To a suspension of [(bmmp-TASN)Fe^{III}Cl]·0.5EtOH (0.10 g, 0.23 mmol) in CH_2Cl_2 (100 mL) was added NEt_4CN (0.050 g, 0.3 mmol) in CH_2Cl_2 (15 mL) dropwise over 10 min with vigorous stirring. The resulting reaction mixture was stirred for 2 h and then filtered. The blue-green filtrate was concentrated to ∼5 mL, and 5 mL of dry ether was added. The blue precipitate thus obtained was filtered, washed with acetonitrile (10 mL) and then with dry ether (20 mL), and vacuum-dried. Yield: 0.065 g (66%). Electronic absorption spectra: (CH_2Cl_2) λ_{max} (ϵ_M) = 660 (sh) (2020), 580 (2740), 455 (1560), 315 (sh) (10100) 265 (13400) nm. IR (KBr) ν (cm^{-1}): 3433

(16) Huang, W.; Jia, J.; Cummings, J.; Nelson, M.; Schneider, G.; Lindqvist, Y. *Structure* **1997**, *5*, 691−699.
(17) Nagashima, S.; Nakasako, M.; Dohmae, N.; Tsujimura, M.; Tokoi, K.; Odaka, M.; Yohda, M.; Kamiya, N.; Endo, I. *Nat. Struct. Biol.* **1998**, *5*, 347−351.
(18) Tsujimura, M.; Dohmae, N.; Odaka, M.; Chijimatsu, M.; Takio, K.; Yohda, M.; Hoshino, M.; Nagashima, S.; Endo, I. *J. Biol. Chem.* **1997**, *272*, 29454−29459.
(19) Murakami, T.; Nojiri, M.; Nakayama, H.; Odaka, M.; Yohda, M.; Dohmae, N.; Takio, K.; Nagamune, T.; Endo, I. *Protein Sci.* **2000**, *9*, 1024−1030.
(20) Green, S. N.; Chang, C. H.; Richards, N. G. J. *Chem. Commun.* **2002**, 2386-2387.
(21) Clairborne, A.; Yeh, J. I.; Mallet, T. C.; Luba, J.; Crane, E. J., III.; Charrier, V.; Parsonage, D. *Biochemistry* **1999**, *38*, 15407−15416.
(22) Mascharak, P. K. *Coord. Chem. Rev.* **2002**, *225*, 201−214.
(23) Noveron, J. C.; Olmstead, M. M.; Mascharak, P. K. *J. Am. Chem. Soc.* **2001**, *123*, 3247−3259.
(24) Tyler, L. A.; Noveron, J. C.; Olmstead, M. M.; Mascharak, P. K. *Inorg. Chem.* **1999**, *38*, 616.
(25) Noveron, J. C.; Herradora, R.; Olmstead, M. M.; Mascharak, P. K. *Inorg. Chim. Acta* **1999**, *285*, 269−276.
(26) Noveron, J. C.; Olmstead, M. M.; Mascharak, P. K. *Inorg. Chem.* **1998**, *37*, 1138.
(27) Shearer, J.; Jackson, H. L.; Schweitzer, D.; Rittenberg, D.; Leavy, T. M.; Kaminsky, W.; Scarrow, R. C.; Kovacs, J. A. *J. Am. Chem. Soc.* **2002**, *124*, 11417−11428.
(28) Schweitzer, D.; Shearer, J.; Rittenberg, D.; Shoner, S. C.; Ellison, J. J.; Loloee, R.; Lovell, S.; Barnhart, D.; Kovacs, J. A. *Inorg. Chem.* **2002**, *41*, 3128−3136.
(29) Jackson, H. L.; Shoner, S. C.; Rittenberg, D.; Cowen, J. A.; Lovell, S.; Barnhart, D.; Kovacs, J. A. *Inorg. Chem.* **2001**, *40*, 1646−1653.
(30) Schweitzer, D.; Ellison, J. J.; Shoner, S. C.; Lovell, S.; Kovacs, J. A. *J. Am. Chem. Soc.* **1998**, *120*, 10996−10997.
(31) Scarrow, R. C.; Strickler, B. S.; Ellison, J. J.; Shoner, S. C.; Kovacs, J. A.; Cummings, J. G.; Nelson, M. J. *J. Am. Chem. Soc.* **1998**, *120*, 9237−9245.
(32) Li, M.; Bonnet, D.; Bill, E.; Neese, F.; Weyermuller, T.; Blum, N.; Sellmann, D.; Wieghard, K. *Inorg. Chem.* **2002**, *41*, 3444−3456.
(33) Grapperhaus, C. A.; Patra, A. K.; Mashuta, M. S. *Inorg. Chem.* **2002**, *41*, 1039−1041.
(34) Mills, D. K.; Font, I.; Farmer, P. J.; Hsiao, Y.-M.; Tuntulani, T.; Buonomo, R.; Goodman, D. C.; Musie, G.; Grapperhaus, C. A.; Maguire, M. J.; Lai, C. H.; Hatley, M. L.; Smee, J. J.; Bellefeuille, J. A.; Darensbourg, M. Y. *Inorg. Synth.* **1998**, *32*, 89−98.
(35) Hoffmann, P.; Steinhoff, A.; Mattes, R. *Z. Naturforsch., B: Chem. Sci.* **1987**, *42b*, 867−873.

(alcohol −OH), 2083 (CN). Anal. Calcd for $C_{16}H_{31}N_3S_3O_{0.5}Fe$: C, 43.53; H, 7.08; N, 9.52. Found: C, 43.81; H, 6.77; N, 9.76.

[(bmmp-TASN)Fe^{III}]$_2$O·H_2O (3). To a suspension of [(bmmp-TASN)Fe^{III}Cl]·0.5EtOH (0.20 g, 0.46 mmol) in CH_2Cl_2 (100 mL) was added NaOH (1.4 g, 25 mmol) in degassed water (5 mL) via cannula under N_2 immediately yielding a dark red solution. The mixture was stirred for 2 h and then separated anearobically. The organic phase was dried over Na_2SO_4 and evaporated in vacuo to yield **3**, a dark red solid (125 mg, 80%). X-ray quality crystals were obtained from CH_2Cl_2/hexane by liquid diffusion. Electronic absorption spectra: (CH_2Cl_2) λ_{max} (ϵ_M) = 529 (6260), 458 (4120), 313 (13900), 230 (19900) nm. IR (KBr) ν (cm^{-1}): 800 (Fe−O−Fe). Anal. Calcd for $C_{28}H_{58}N_4S_6O_2Fe_2$: C, 42.74; H, 7.43; N, 7.12. Found: C, 42.23; H, 7.14; N, 6.92.

[(bmmp-TASN)Zn] (5). To a solution of H_2[(bmmp-TASN)]·2HCl (0.70 g, 2.0 mmol) in degassed methanol (35 mL) mixed with 1.5 mL of NEt_3 was added a solution of anhydrous zinc chloride (0.21 g, 1.6 mmol) in methanol (15 mL) via cannula. The resultant solution was stirred overnight and evaporated in vacuo to yield a white solid, which was washed with water and ether to yield 61 mg of **5**. Anal. Calcd for $C_{14}H_{28}N_2S_3Zn$: C 42.57, H 7.34, N 7.09. Found: 42.46, 6.98, 6.91.

Physical Methods. Elemental analyses were obtained from Midwest Microlab (Indianapolis, IN) or Galbraith Laboratories, Inc. (Knoxville, TN). IR spectra were recorded on a Thermo Nicolet Avatar 360 spectrometer at 4 cm^{-1} resolution. Electronic absorption spectra were recorded with an Agilent 8453 diode array spectrometer with 1 cm path length quartz cells. ^{1}H NMR spectra were obtained on a Varian Inova500 500-MHz spectrometer. X-band EPR spectra were obtained on a Bruker EMX EPR spectrometer at 77 K in a Suprasil quartz dewar. Cyclic voltammetric measurements were performed by using a PAR 273 potentiostat with a three-electrode cell (glassy carbon working electrode, platinum wire counter electrode, and Ag/AgCl reference electrode) at room temperature.

Crystallographic Studies. Crystals were mounted on a 0.05 mm CryoLoop with Paratone oil for collection of X-ray data using a Bruker SMART APEX CCD diffractometer. For each structure, the SMART[36] software package (v 5.625) was used to acquire a total of 1868 30-s frame exposures of data at 100 K using monochromated Mo Kα radiation (0.71073 Å) from a sealed tube and a monocapillary. Frame data were processed using SAINT[37] (v 6.22) to produce the raw *hkl* data, which were then corrected for absorption using SADABS[38] (v 2.02). Structures were solved by direct methods using SHELXS-90[39] and refined by least-squares methods on F^2 using SHELXL-97[40] incorporated into the SHELXTL[41] (v 6.12) suite of programs.

A purple plate (0.28 × 0.20 × 0.03 mm) crystal of **3** was obtained by liquid diffusion of hexane into a methylene chloride solution of the complex at room temperature. A disordered CH_2Cl_2 solvate was present and modeled as two half-occupancy Cl−C−Cl groups each of 50% occupancy; hydrogens of the methylene chloride were excluded. All non-hydrogen atoms were refined anisotropically. H atom positions were calculated and were allowed to ride on the carbon atom to which they were attached by refining the torsion angle that defines its orientation. Thermal values were assigned U(H) = 1.2 and 1.5U_{eq} attached C, for methylene and methyl hydrogens, respectively. For all 4592 unique reflections (R(int) = 0.016) the final anisotropic full matrix least-squares refinement on F^2 for 245 variables converged at R1 = 0.031 and wR2 = 0.065 with a GOF of 1.01. Details of data collection, structure solution, and refinement are given in Table 1.

Table 1. Crystal Data and Structure Refinement for **3** and **5**

	3	**5**
empirical formula	$C_{28}H_{56}Fe_2N_4OS_6$·CH_2Cl_2	$C_{14}H_{28}N_2S_3Zn$·$1H_2O$·CH_2Cl_2
fw	853.78	488.88
temp (K)	100(2)	100(2)
wavelength (Å)	0.71073	0.71073
cryst syst	triclinic	monoclinic
space group	$P\bar{1}$	$P2_1/n$
unit cell dimens		
a (Å)	10.5486(15)	9.5759(6)
b (Å)	13.0612(19)	20.9790(13)
c (Å)	8.1852(12)	10.7113(7)
α (deg)	96.923(2)	
β (deg)	112.729(2)	91.283(1)
γ (deg)	81.048(2)	
volume (Å^3)	1025.2(3)	2151.3(2)
Z	1	4
density (Mg/m^3) (calcd)	1.514	1.509
abs coeff (mm^{-1})	1.305	1.688
cryst size (mm^3)	0.28 × 0.20 × 0.03	0.35 × 0.11 × 0.07
cryst color, habit	purple plate	colorless needle
θ range for data collection (deg)	2.11−28.25	1.94−28.30
index ranges	$-13 \le h \le 13$ $-16 \le k \le 17$ $-10 \le l \le 10$	$-12 \le h \le 12$ $-27 \le k \le 27$ $-14 \le l \le 14$
reflns collected	9074	18696
indep reflns	4592 [R(int) = 0.016]	4996 [R(int) = 0.030]
completeness to θ = 28.25°	90.8%	93.4%
abs correction	SADABS	SADABS
min and max transm	0.738 and 0.962	0.800 and 0.881
refinement meth	full-matrix least-squares on F^2	
data/restraints/params	4592/0/245	4996/0/259
GOF on F^2	1.01	1.04
final R indices [$I > 2\sigma(I)$][a,b]	R1 = 0.027, wR2 = 0.064	R1 = 0.027, wR2 = 0.061
R indices (all data[a,b])	R1 = 0.031, wR2 = 0.065	R1 = 0.036, wR2 = 0.063
largest peak and hole (e·Å^{-3})	0.713 and −0.384	0.458 and −0.251

[a] $R1 = \sum||F_o| - |F_c||/\sum|F_o|$. [b] $wR2 = \{\sum[w(F_o^2 - F_c^2)^2]/\sum[w(F_o^2)^2]\}^{1/2}$.

A colorless needle (0.35 × 0.11 × 0.07 mm) crystal of **5** was obtained by liquid diffusion of hexane into a methylene chloride solution of the complex at room temperature. All non-hydrogen atoms were refined anisotropically. Methyl and methylene hydrogen atoms (including the CH_2Cl_2 solvate) were placed in their geometrically generated positions and refined by allowing their coordinates to ride on the carbon atom to which they are attached. Hydrogen atoms of the water molecule were located by difference maps and their positions were refined. Thermal values U(H) for all hydrogen atoms were refined. For all 4996 unique reflections (R(int) = 0.030) the final anisotropic full matrix least-squares refinement on F^2 for 259 variables converged at R1 = 0.036 and wR2 = 0.063 with a GOF of 1.04. Details of data collection, structure solution, and refinement are given in Table 1.

(36) *SMART*, v5.625; Bruker Advanced X-ray Solutions, Inc.: Madison, WI, 2001.

(37) *SAINT*, v6.22; Bruker Advanced X-ray Solutions, Inc.: Madison, WI, 2001.

(38) Sheldrick, G. M. *SADABS (v2.02), Area Detector Absorption Correction*; University Göttingen: Göttingen, Germany, 1997.

(39) Sheldrick, G. M. SHELXS-90. *Acta Crystallogr.* **1990**, *A46*, 467−473.

(40) Sheldrick, G. M. *SHELXL-97, Program for the Refinement of Crystal Structures*; University of Göttingen: Göttingen, Germany, 1997.

(41) *SHELXTL (v6.12), Program Library for Structure Solution and Molecular Graphics*; Bruker Advanced X-ray Solutions, Inc.; Madison, WI, 2001.

Scheme 1

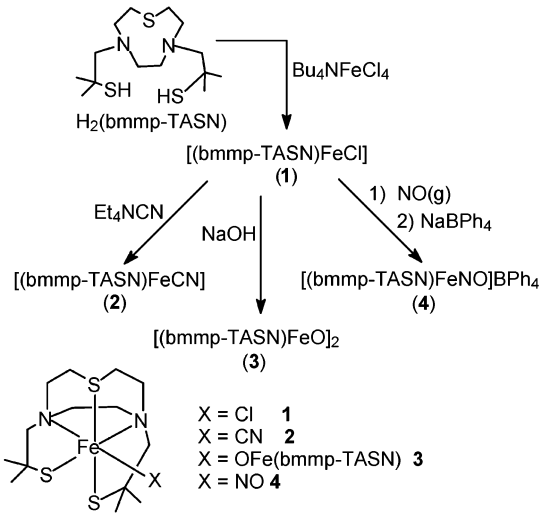

Additional details including atomic coordinates and anisotropic displacement parameters as well as complete lists of bond lengths, angles, and torsion angles are available in the Supporting Information in CIF format.

Results

Syntheses and Characterization. A series of iron complexes based on the pentadentate ligand H_2(bmmp-TASN) were synthesized and isolated as shown in Scheme 1. As isolated, the (chloro)iron(III) complex [(bmmp-TASN)-$Fe^{III}Cl$] (**1**) is of suitable purity for preparation of the other iron derivatives. Although in solution the bound chloride of **1** is readily exchangeable, conductivity measurements in dichloromethane confirm that **1** is a nonelectrolyte in solution. Addition of a slight excess (1.4 equiv) of Et_4NCN to dark blue solutions of **1** in dichloromethane yields [(bmmp-TASN)$Fe^{III}CN$] (**2**) as a blue solid following filtration and precipitation. Like **1**, **2** is a nonelectrolyte in solution. The infrared spectrum of **2** displays a single ν_{CN} stretch at 2083 cm^{-1}. Addition of 1.4 equiv of NBu_4OH to **1** in CH_2Cl_2, in the presence or absence of nitriles, yields a deep violet solution, from which crude **3** is obtained as a violet powder. Pure **3** is obtained using NaOH as the base, allowing isolation of single crystals of the oxo-bridged product, [(bmmp-TASN)$Fe^{III}O]_2$ (**3**), suitable for X-ray analysis. Complex **3** displays an intense stretching frequency at 799 cm^{-1} typical of oxo-bridged diiron complexes. As preliminarily reported, **1** reacts with nitric oxide in acetonitrile solution to yield [(bmmp-TASN)$Fe^{III}NO]^+$, which is isolated in crystalline form as the BPh_4^- salt, **4**.[33] The X-ray structure, Mössbauer spectrum, and IR spectrum of **4** have previously been reported. The zinc complex, (bmmp-TASN)-Zn^{II} (**5**), was obtained directly from the HCl salt of H_2(bmmp-TASN) and zinc chloride.

The X-band EPR spectra of complexes **1** and **2** as dilute, frozen solutions were obtained at 77 K, Figure S1 and S2 (Supporting Information). The chloro derivative **1** displays a single, intense line at $g = 4.28$ consistent with a high-spin ($S = {}^5/_2$) ground state in a rhombic environment. The cyano complex **2** displays a rhombic signal with g-values near 2.00 consistent with a low-spin ($S = {}^1/_2$) ground state: $g_1 = 2.31$, $g_2 = 2.16$, and $g_3 = 1.96$. Analysis of the g-values using the method of Griffith, and expanded by Taylor, finds the unpaired electron primarily, >99%, in the d_{xy} orbital.[42,43] The d_{xy}, d_{xz}, and d_{yz} orbitals are split by a strong tetragonal component, $|\Delta/\lambda| = 9.30$, and a large rhombic component, $|\Delta/\lambda| = 5.38$. Frozen dichloromethane solutions of **3** (77 K) display only a residual signal of **1**, consistent with an antiferromagnetically coupled diiron(III) μ-oxo complex, Figure S3 (Supporting Information).

As previously reported, the nitrosyl complex, **4**, has an $S = 0$ ground state consistent with its formulation as an {Fe-NO}^{6} complex using the notation of Enemark and Feltham.[44] The ^{1}H NMR spectrum of **4**, Figure S4 (Supporting Information), displays a series of multiplets between 3.05 and 4.85 ppm associated with the 16 protons of the TASN backbone and the methylene protons of the thiolate sidearms. Four methyl resonances between 1.41 and 1.66 ppm are observed. The zinc complex, **5**, displays a similar, although less complex, spectrum with methyl resonances at 1.35 and 1.39 ppm (12 H), a doublet at 2.53 ppm (2 H), a multiplet between 2.68 and 2.88 ppm (12 H), and a multiplet at 3.50 ppm (2 H), Figure S5 (Supporting Information).

The iron complexes **1**−**4** range in color from dark blue to deep violet. In each complex, the lowest energy band is assigned as in related Fe(III)−thiolate complexes to a thiolate to iron transfer band from the lone pair (p) orbital on the ligand to the iron d orbitals.[29] This band occurs at slightly lower energy in the low-spin complexes, 15200 and 15400 cm^{-1} for **2** and **4**, respectively, than in the high-spin derivatives, 16000 and 19000 cm^{-1} for **1** and **3**, respectively. The high-spin complexes also display a pair of bands near 22100 and 31000 cm^{-1}. In addition to the thiolate to metal charge-transfer band, the low-spin complexes, **2** and **4**, display a second lower energy band, 17200 and 18700 cm^{-1}. The difference in energy between the first and second transition in the nitrosyl complex, 3300 cm^{-1} or 0.41 eV, is similar to the calculated difference in energy between the HOMO and HOMO−1 of 0.32 eV; both of which contain significant sulfur p-character (vide infra).

Complex **4** was subjected to photolysis under a variety of conditions. Either a tungsten bulb (60 W) or mercury vapor lamp (medium pressure) was used as the light source. For each light source, the solvents were varied from acetonitrile, to dichloromethane, to dimethylformamide. Solvents were degassed via freeze−pump−thaw (three cycles) prior to photolysis, up to 48 h, in a sealed Schlenk flask (Pyrex). Only under prolonged photolysis in DMF with a Hg-vapor lamp was loss of NO-coordination and color change of the solution observed, although this result was not always reproducible. Similar results, including the IR spectrum of isolated decomposition product, were obtained in the dark under aerobic conditions, suggesting that, during prolonged conditions, O_2 may leach into the system, leading to oxidative

(42) Griffith, J. S. *Proc. R. Soc. London, A* **1956**, *235*, 23−36.
(43) Taylor, C. P. S. *Biochim. Biophys. Acta* **1977**, *491*, 137.
(44) Enemark, J. H.; Feltham, R. D. *Coord. Chem. Rev.* **1974**, *13*, 339−406.

Table 2. Electrochemical Data[a] from Cyclic Voltammetry in CH_2Cl_2[b] for **1**−**5**

complex	E_{red}, V (ΔE_p)	E_{ox}[c], V
1	−0.66[c]	+0.58
2	−0.88 (120)	+0.29
3	−0.67	+0.66
4	−0.234 (120)	+0.96
	−1.25 (260)	
5		+0.96

[a] All potentials are measured at a scan rate of 200 mV/s at a glassy carbon electrode referenced to Ag/AgCl. [b] ∼1 mM solutions with 0.1 M TBAHFP as supporting electrolyte. [c] The process is irreversible. The potential recorded is E_{pc} (reductions) or E_{pa} (oxidations) measured at 200 mV/s.

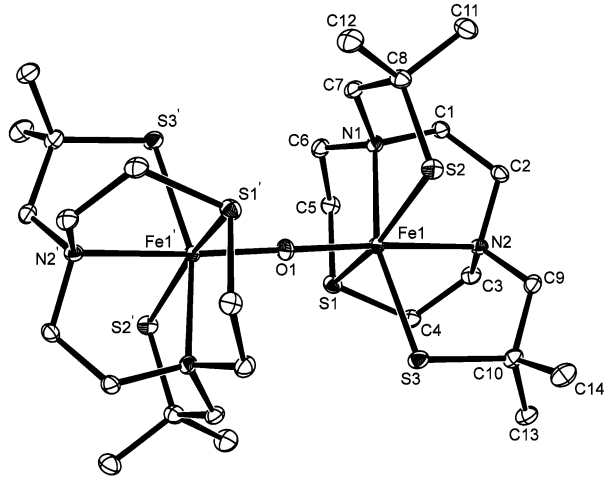

Figure 1. ORTEP view of **3** showing 30% probability displacement ellipsoids and the atom-numbering scheme. H atoms and the solvent molecule are omitted.

decomposition. There is no evidence of photolytic Fe−NO bond cleavage of **4**.

Electrochemical Investigations. Results of cyclic voltammetry studies of **1**−**5** in dichloromethane solution are summarized in Table 2. All potentials are referenced versus Ag/AgCl. Each of the complexes, including the zinc derivative, displays an irreversible oxidation ranging from +0.29 to +0.96 V assigned as a thiolate (RS^-) to thiyl ($RS^\bullet$) sulfur-centered oxidation. In addition, the two high-spin iron complexes, **1** and **3**, display a quasi-reversible reduction with E_{pc} values of −0.66 and −0.67 V, respectively, assigned as an $Fe^{III/II}$ couple. The low-spin cyano complex, **2**, is more difficult to reduce, −0.88 V, but the event occurs reversibly. The nitrosyl complex, **4**, displays a pair of reversible reductions at −0.23 and −1.25 V assigned to $\{Fe\text{-}NO\}^{6/7}$ and $\{Fe\text{-}NO\}^{7/8}$ redox couples.

X-ray Crystal Structure Determinations. The structures of complexes **3**−**5** have been determined by single-crystal X-ray techniques. The nitrosyl complex, **4**, has previously been reported. Details of the data collection and refinement of **3** and **5** are presented in Table 1.

Complex **3** crystallizes with one dichloromethane solvent molecule as purple plates. A molecular view of **3** is presented in Figure 1 with selected bond distances and bond angles listed in Table 3.[45] In **3**, the TASN backbone (N1, N2, S1) occupies one face of the pseudo-octahedron around iron with the pendant thiolate donors S2 and S3 located at positions

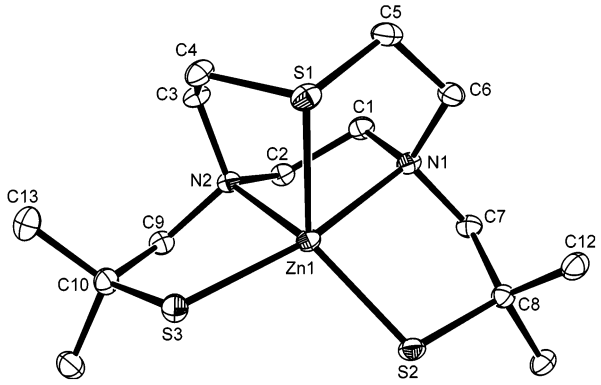

Figure 2. ORTEP view of **5** showing 50% probability displacement ellipsoids and the atom-numbering scheme. H atoms and the solvent molecules are not shown.

Table 3. Selected Bond Distances (Å) and Bond Angles (deg) for $[(bmmp\text{-}TASN)Fe]_2O$ (**3**)

Fe1−S1	2.6221(6)	Fe1−S2	2.3970(5)
Fe1−S3	2.3374(5)	Fe1−N1	2.297(1)
Fe1−N2	2.377(1)	Fe1−O1	1.7954(3)
N1−Fe1−N2	75.35(5)	N1−Fe1−S1	78.25(4)
N2−Fe1−S1	78.23(3)	N1−Fe1−S2	82.34(4)
N2−Fe1−S3	80.82(4)	S2−Fe1−S3	102.54(2)
O1−Fe1−S2	102.02(2)	Fe1−O1−Fe1′	180.0

Table 4. Selected Bond Distances (Å) and Bond Angles (deg) for (bmmp-TASN)Zn (**5**)

Zn1−S1	2.4513(5)	Zn1−S2	2.2808(5)
Zn1−S3	2.3688(5)	Zn1−N1	2.3607(14)
Zn1−N2	2.1479(14)		
N1−Zn1−N2	78.91(5)	N1−Zn1−S1	81.08(3)
N2−Zn1−S1	88.89(4)	N1−Zn1−S2	85.63(3)
N2−Zn1−S3	86.11(4)	S2−Zn1−S3	105.03(2)

trans to S1 and N1, respectively. The Fe−N bond distances of 2.297(1) and 2.377(1) Å to N1 and N2, respectively, are typical for octahedral high-spin iron(III). The relatively long Fe−S1 distance of 2.6221(6) Å is similar to that of the *high-spin* complex $(TASN)FeCl_3$, 2.549(1) Å.[46] The TASN ring constrains the N1−Fe1−N2 angle to 75.35(5)° as seen in related complexes. The N1−Fe1−S1, 78.25(4)°, and N2−Fe1−S1, 78.23(3)°, bond angles are similarly constrained. The Fe−S bond distances to the anionic, thiolate sulfurs of 2.3970(5) and 2.3377(5) Å to S2 and S3, respectively, are significantly shorter than the neutral, thioether to iron distance, Fe−S1. The coordination sphere about iron is completed by the bridging oxygen, O1, located on an inversion center which symmetrically generates the μ-oxo complex with an Fe1−O1−Fe1′ bond angle of 180.00°. The Fe1−O1 bond distance is expectedly short, 1.7954(3) Å.

Complex **5** crystallizes as colorless needles with one water and one dichloromethane molecule of solvation, Figure 2. Selected bond angles and distances are provided in Table 4. The zinc sits in a distorted N_2S_3 donor environment with a τ value of 0.46, intermediate between that of a square pyramidal ($\tau = 0.0$) and a trigonal bipyramidal ($\tau = 1.0$) geometry.[47] This results in asymmetric Fe−N and Fe−S bond

(45) Farrugia, L. J. ORTEP-3 for Window. *J. Appl. Crystallogr*. **1997**, *30*, 565.
(46) Grillo, V. A.; Hanson, G. R.; Hambley, T. W.; Gahan, L. R.; Murray, K. S.; Moubaraki, B. *J. Chem. Soc., Dalton Trans.* **1997**, 305−311.

Table 5. Comparison of Calculated and Experimental Bond Distances (Å) and Bond Angles (deg) for **4**

	calcd	exptl[a]
$Fe-S_{thiolate}$	2.313, 2.326	2.284(2), 2.291(2)
$Fe-S_{thioether}$	2.342	2.285(2)
$Fe-N_{amine}$	2.066, 2.096	2.024(5), 2.063(5)
$Fe-N_{NO}$	1.616	1.609(6)
N−O	1.148	1.167(6)
Fe−N−O	174.51	177.2(6)
$S_{thiolate}-Fe-S_{thioether}$	89.02, 174.24	89.91(7), 175.81(8)
$N_{amine}-Fe-N_{NO}$	171.26, 103.07	175.4(3), 98.7(3)

[a] Reference 33.

distances consistent with N1 and S3 sitting in the "axial" positions and N2, S1, and S2 sitting in the "equatorial" positions of a distorted trigonal bipyramidal geometry. The Zn−N1 and Zn−N2 bond lengths are 2.361(1) and 2.148(1) Å, respectively. Likewise, the thiolate to zinc bond lengths are 2.281(1) and 2.369(1) Å to S2 and S3. The thioether−zinc bond distances is slightly longer, 2.451(1) Å. The steric requirements of the facially coordinating TASN ring prevent a true trigonal bipyramidal arrangement. The angles between zinc and the TASN donor atoms are all acute, as in the iron derivative: N1−Zn−N2, 78.91(5)°; N1−Zn−S1, 81.08(3)°; N2−Zn−S1, 88.89(4)°. Neighboring zinc-centers in the crystal are linked via a weak hydrogen-bonding network between S3, O1, and S2′ with a S3···O1 distance of 3.290 Å, a S3−H2−O1 angle of 162.96°, an S2′···O1 distance of 3.299 Å, and an S2′−H2−O1 angle of 174.63°.

Theoretical Investigations

The B3LYP exchange-correlation functional with the 6-31g(d) basis set was employed to optimized the structure of **4**.[48] The Gaussian 98 suite of programs was used for electronic structure calculations with full population analysis of the molecular orbitals. A comparison of theoretical and experimental bond distances and angles is provided in Table 5. The calculated structure slightly (0.03−0.06 Å), but consistently, overestimates the metal−ligand bond distances to bmmp-TASN. It also accurately reproduces the iron−nitrosyl bond distances and angles.

Figure 3 shows relative orbital energies and a representation of the HOMO and LUMO of **4**. As in similar nickel−thiolate complexes, this orbital is largely centered on a sulfur-p lone pair, which is out of phase with a metal-centered d orbital.[49] The nucleophilicity of metal-coordinated thiolates has been attributed to this four-electron antibonding interaction between the filled metal d orbital and sulfur p orbital.[50] The HOMO−1 orbital, not shown, is a similar interaction between the other thiolate sulfur and a metal d orbital. In fact, metal sulfur interactions dominate the occupied frontier orbitals. The Fe−NO π-back-bonding orbital (HOMO−5), the anticipated HOMO in iron−nitrosyl complexes, lies

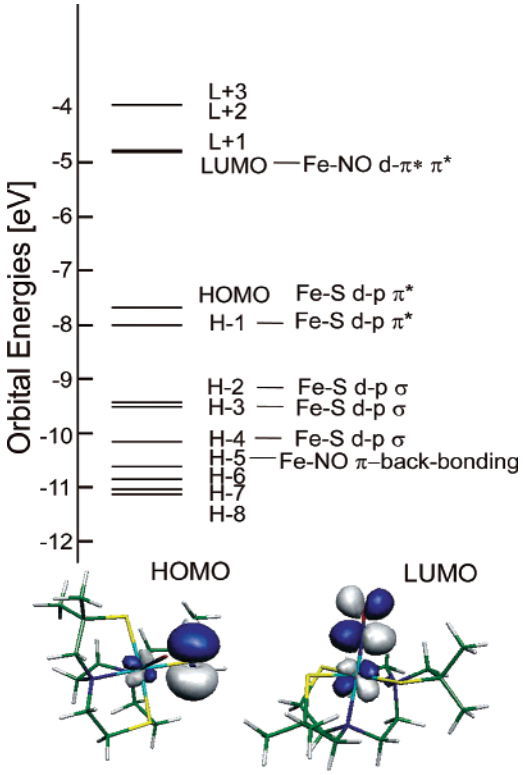

Figure 3. Calculated energy level diagram of **4** including representations of the HOMO (bottom left) and LUMO (bottom right).

∼2.94 eV below the HOMO in **4**. The LUMO orbital, Figure 3 (bottom, right), is a π-antibonding interaction between the metal and the nitrosyl. Bending, computationally, of the Fe−N−O bond decreases the HOMO−LUMO gap by lowering the energy of the LUMO orbital as a result of the decreased π-overlap. The calculated HOMO−LUMO gap decreases from 2.63 eV for a linear (174.5°) Fe−N−O bond angle to 2.19 and 1.73 eV for angles of 160° and 145°, respectively.

Discussion/Relevance to Nitrile Hydratase

The N_2S_3 pentadentate ligand, $(bmmp\text{-}TASN)^{2-}$, contains a facial coordinating N_2S TASN ring that positions two thiolato donors in positions cis to one another upon coordination. The ligand binds iron(III) with a single, variable additional ligand, X. As demonstrated by EPR and NMR, the nature of X, and not the presence of the two π-donating thiolate donors, determines the spin state of the complex. Low-spin complexes result when X is a π-accepting ligand (CN^-, NO), while π-donors (Cl^-, O^{2-}) yield high-spin complexes. A qualitative MO diagram (Figure S6) and discussion are provide in the Supporting Information. In the native enzyme, the iron remains low-spin regardless of the nature of X. This can be attributed, in part, to the stronger donor ability of deprotonated amides as compared to amines yielding a larger "t_{2g}"−"e_g" gap. Additionally, S-oxygenates removes π-donor character from two of the three sulfur donors, which would also favor low-spin complexes. We have reported previously in communication form that **4** serves as both a structural and spectroscopic mimic of NO-inactivated NHase even without inclusion of amido N-donors.[33]

(47) Addison, A. W.; Rao, T. N.; Reedijk, J.; van Rijn, J.; Verschoor, G. C. *J. Chem. Soc., Dalton Trans.* **1984**, 1349−1356.
(48) (a) Becke, A. D. *J. Chem. Phys.* **1993**, *98*, 5648. (b) Lee, C.; Yang, W.; Parr, R. G. *Phys Rev.* **1988**, *B37*, 785 (B3LYP/6-31G*).
(49) Kaasjager, V. E.; Bouwman, E.; Gorter, S.; Reedijk, J.; Grapperhaus, C. A.; Reibenspies, J. H.; Smee, J. J.; Darensbourg, M. Y.; Derecskei-Kovacs, A.; Thomson, L. M. *Inorg. Chem.* **2002**, *41*, 1837−1844.
(50) Grapperhaus, C. A.; Darensbourg, M. Y. *Acc. Chem. Res.* **1998**, *31*, 451−459.

With respect to structural modeling, the metric data of **3** and **4** highlight an important key difference between high-spin and low-spin iron−thiolate bonding. As expected, the metal−ligand bond distances are shorter in the low-spin iron complex, **4**, than in the high-spin complex, **3**. For the σ-only ligands, N1, N2, and S1, the difference in bond lengths is relatively constant, 27, 31, and 34 pm even though N2 is trans to X, the nature of which changes from π-donating to π-accepting from **3** to **4**. However, the decrease in the Fe−thiolate bond distances is significantly less, 5−10 pm, than the σ-only donors. This can be attributed to a "lengthening" of the Fe−thiolate bond distance in the low-spin complexes as a result of four-electron π-repulsion between the S lone pair and the iron "t_{2g}" electrons.[51] Interestingly, the Fe−S bond distance for low-spin iron is nearly identical for thiolate (anionic) and thioether (neutral) donors as a result. The same trend holds for Ru(III) complexes that contain both thiolate and thioether donors.[52] For high-spin iron(III), the "t_{2g}" orbitals are only half-occupied. This, coupled with the larger ionic radii of high-spin versus low-spin iron, significantly decreases the π-repulsion between the metal and the ligand. As a result, the iron−thiolate and iron−thioether bond distances are statistically quite different for high-spin iron(III). Thus, we previously posed the question, "Are thiolate and thioether donors equivalent for low-spin iron complexes?" As reported in communication form, the answer is *yes* when *structural equivalency* is discussed, but a resounding *no* from an *electronic equivalency* viewpoint due to the significant difference in orbitals involved in metal−sulfur bonding (vide supra).[33]

Iron-containing nitrile hydratase displays a characteristic band at 710 nm (14100 cm^{-1}) that has been assigned as a thiolate to iron charge-transfer band that is often a target for model complexes.[5] Complexes **1**−**4** display similar charge transfer bands, at slightly higher energies, in the UV−visible spectrum at 16000, 15200, 19000 and 15400 cm^{-1}, respectively. As the thiolate to metal charge-transfer represents transfer of electron density from sulfur to iron, in an extreme limiting case it could be regarded as ligand oxidation coupled with a metal reduction ($RS^{-}-Fe^{III} \rightarrow RS^{\bullet}-Fe^{II}$). Hence, the energy of the charge-transfer band is related to the difference in potential between the thiolate oxidation and metal reduction, not their absolute values. While the reduction potentials of the high-spin **1** and low-spin **4** differ by ∼300 mV, the oxidation potentials are similarly shifted and the energies of the charge-transfer bands are nearly equivalent. Likewise, the high-spin complexes **1** and **3** have nearly equivalent reduction potentials, but differences in their oxidation potentials result in significant differences in the energy of the charge-transfer band. Thus the charge-transfer band is not a reliable indicator of how well a model reproduces the absolute electronic environment of the enzyme, but rather a measure of how well it separates the oxidized and reduced forms of the complex. For hydrolytic enzymes, such as NHase, it may be more appropriate to compare reduction potentials of models as indicators of the Lewis acidity of the metal center rather than relying on the UV−visible spectrum. In this respect, the high-spin complexes **1** and **3** accurately mimic the $Fe^{III/II}$ reduction potential of NHase (−480 mV vs NHE; Ag/AgCl vs NHE = 0.197 V).[5]

Interestingly, the inclusion of amine instead of amido nitrogen donors and a single thioether donor in the N_2S_3 donor set does not preclude these complexes from serving as spectroscopic mimics of iron-containing NHase. The similarity in donor ability of these two sets arises, at least in part, from the comparable donor ability of thioethers and sulfur−oxygenates. When comparing thiolates and thioethers, the thiolate is clearly the stronger σ-donor. Sulfur−oxygenates are somewhere in between these two extremes, as the donor is still formally anionic although the oxygen atoms withdraw electronic density away from the sulfur. In terms of π-interactions, the thiolate serves as π-donor, which causes an antibonding interaction with the metal in the case of low-spin iron, whereas for thioethers there is no π-interaction between the metal and the ligand. Likewise, upon S-oxygenation, no sulfur lone pair is available for π-interactions with the metal. *Thus when S-oxygenated cysteine residues (moderate σ-donor, π-neutral) are modeled, thioethers (weaker σ-donor, π-neutral) more closely mimic the nature of the M−S bond than thiolates (stronger σ-donor, π-donor).*

Although we suggest thioethers are *better* mimics of S-oxygenates than thiolates, it is not insinuated that S-oxygenates and thioethers are *identical* donors. While **4** reproduces key structural and electronic features of NO-inactivated NHase, the Fe−NO bond of the former is not cleaved upon photolysis. This is consistent with subtle, yet vital changes in the electronic transitions of absorption peaks in oxygenated versus non-oxygenated NHase recently reported by Richards et al. that may not be reproduced by the thioether.[20] Alternately, the lack of NO photolability may arise from the absence of a suitably strong trans donor.[53] Additionally, the thioether fails to mimic any steric or H-bonding role that the S-oxygenate may serve at the active site. Clearly, these factors may be significant in controlling activity, either hydrolytic or photolytic, at the iron site. The preparation of a functional, as opposed to structural or electronic, model of nitrile hydratase may require incorporation of a "second-coordination sphere" scaffold to reproduce these effects and prevent μ-oxo dimer formation while facilitating deprotonation of metal-coordinated water.

Acknowledgment is made to the donors of the Petroleum Research Fund, administered by the ACS, for partial support of this research (ACS PRF#37663-G3). We thank the Kentucky Research Challenge Trust Fund for the purchase of CCD X-ray equipment and upgrade of our X-ray facility.

Supporting Information Available: EPR spectra of **1**−**3**, ^1H NMR spectra of **4**−**5**, a qualitative MO diagram, and crystallographic data in CIF format. This material is available free of charge via the Internet at http://pubs.acs.org.

IC026239T

(51) Ashby, M. T.; Enemark, J. H.; Lichtenberger, D. L. *Inorg. Chem.* **1988**, *27*, 191−197.

(52) Grapperhaus, C. A.; Poturovic, S.; Mashuta, M. S. *Inorg. Chem.* **2002**, *41*, 4309−4311.

(53) Patra, A. K.; Afshar, R.; Olmstead, M. M.; Mascharak, P. K. *Angew. Chem., Int. Ed.* **2002**, *41*, 2512−2515.